

## Consideration of the Pressure Entrance Loss for the Analysis of Rotordynamic Gas Seals Forces

### **Boris Grigoriev**

Saint-Petersburg State  
Polytechnical University  
195251 Saint-Petersburg, Russia  
grig@tu.neva.ru

### **Joachim Schmied**

DELTA JS AG  
CH-8005 Zurich, Switzerland  
jschmied@delta-js.ch

### **Alexander Fedorov**

Saint-Petersburg State  
Polytechnical University  
195251 Saint-Petersburg, Russia  
aleksandr\_fm1@mail.ru

### **Sergey Lupuleac**

Saint-Petersburg State  
Polytechnical University  
195251 Saint-Petersburg, Russia  
lupuleac@ipc.amd.stu.neva.ru

### **ABSTRACT**

Sophisticated methods (CFD analyses) are used more and more for the analysis of gas seal forces. However, for some types of seals such as honeycomb or hole pattern seals bulk-flow models are still the only feasible way. Ha and Childs introduced such a model in their paper [4]. The entrance loss factor in their model is constant, what apparently leads to an incomplete consideration of the Lomakin effect. Comparison to measured results shows considerable deviation for the radial forces in annular gas seal.

The present paper is dedicated to investigation of the cause of this deviation. For this purpose an extended model for entry conditions is proposed. The entrance loss factor is considered as a function of the seal clearance. Numerical computations of the pressure loss at the entrance of the gas seal using the FLUENT code are performed. The seal gap and the surrounding zones are considered in the solution of the Reynolds-averaged Navier-Stokes system with  $k-\omega$  turbulence model.

The obtained results are used as the boundary conditions for the bulk-flow seal model. This technique improves the algorithm for finding the basic characteristics of the seal, leading to better coincidence of calculated and experimental results. In particular it improves such important parameter as the direct stiffness.

### **KEY WORDS**

Annular Gas Seal, Entrance-Loss Coefficient, CFD-Modeling.

### **1 INTRODUCTION**

Various types of seals are used in turbomachines to limit leakage between regions with different pressures. In practice, some vibration problems were eliminated with annular honeycomb-stator seals. As related to rotor dynamics, seal analysis has the objective of determining the reaction force acting on the rotor as a result of the shaft motion. For small motion about a centered position, the relation between the reaction-force components and the shaft motion can be written as

$$-\begin{pmatrix} F_x \\ F_y \end{pmatrix} = \begin{pmatrix} K & k \\ -k & K \end{pmatrix} \begin{pmatrix} X \\ Y \end{pmatrix} + \begin{pmatrix} C & c \\ -c & C \end{pmatrix} \begin{pmatrix} \dot{X} \\ \dot{Y} \end{pmatrix}. \quad (1)$$

Here  $X$  and  $Y$  are the displacement components of the seal rotor relative to the stator;  $F_x$  and  $F_y$  are the components of the reaction force acting on the rotor. The direct stiffness  $K$ , cross-coupled stiffness  $k$ , direct damping  $C$ , and cross-coupled damping  $c$  are referred as rotor dynamic coefficients.

Nelson [1] developed the governing equations for surface-roughened annular gas seals based on Hirs's turbulent bulk-flow model [2]. Nelson uses fully developed flow friction factor throughout the seal. An abrupt loss at the seal entrance models the high friction in the developing flow region of the seal. In another bulk-flow gas seal analysis, Elrod et al. [3] entrance and exit region friction factor models based on tests of smooth- and honeycomb-stator seals are used. Ha and Childs [4] proposed modeling the fluid within the seal in a two-control-volume fashion. Subsequently, Kleynhans and Childs [5] developed a new analytical technique for determining dynamic coefficients of the seal based on the two-control-volume model. This analysis used a conventional control volume for the through flow of the fluid and a "capacitance accumulator" model for the individual honeycomb cell. The control volume for the honeycomb cell drops the acoustic velocity of the main fluid flow within the frequency range of interest in rotordynamics, thus causing the dynamic coefficients to become frequency dependent.

The above theories predict generally well the gradient pressure, seal leakage and direct damping. However, the cross-coupled stiffness and especially the direct stiffness are predicted poor. The present paper introduces an extension of Ha and Childs model leading to better prediction of direct stiffness. The modeling procedure is divided into two parts. In the first part the Reynolds-averaged Navier-Stokes equations with  $k-\omega$  turbulence model are used to determine the pressure drop on the entrance of the seal. In the second part the two-control volume bulk flow model is applied with regard to computed input pressure drop coefficient.

## 2 GOVERNING EQUATIONS

Let us introduce dimensionless parameters (the bar above the variable points out the dimension values)

$$p = \frac{\bar{p}}{p_{in}}, \quad h = \frac{\bar{h}}{c_0}, \quad u = \frac{\bar{u}}{u_m}, \quad w = \frac{\bar{w}}{u_m}, \quad z = \frac{\bar{z}}{L}, \quad t = \bar{t}\omega, \quad (2)$$

where  $p$  is gas pressure;  $p_{in}$  is reservoir pressure;  $h$  is seal clearance;  $c_0$  is nominal radial clearance;  $u$  and  $w$  is bulk-flow fluid velocity components in circumferential direction  $\varphi$  and axial one  $z$ ;  $u_m = \sqrt{R_g T}$  is isothermal sonic speed ( $R_g$  – gas constant,  $T$  – temperature);  $L$  is seal length;  $\omega$  is shaft rotational velocity.

The dimensionless transformed version of governing equations of the two-control-volume model for annular gas seal has the following form.

Continuity equation

$$S \frac{\partial}{\partial t} p(h + h_d) + 2\beta \frac{\partial}{\partial \varphi} (puh) + \frac{\partial}{\partial z} (pwh) = 0, \quad (3)$$

where  $h_d$  is the honeycomb cell depth,

Axial-Momentum Equation

$$S \frac{\partial w}{\partial t} + 2\beta u \frac{\partial w}{\partial \varphi} + w \frac{\partial w}{\partial z} + \frac{1}{p} \frac{\partial p}{\partial z} = -(\tau_{sz} + \tau_{rz}), \quad (4)$$

Circumferential-Momentum Equation

$$S \frac{\partial u}{\partial t} + 2\beta u \frac{\partial u}{\partial \varphi} + w \frac{\partial u}{\partial z} + 2\beta \frac{1}{p} \frac{\partial p}{\partial \varphi} = -(\tau_{s\varphi} + \tau_{r\varphi}), \quad (5)$$

Wall shear-stresses  $\tau_{ij}$  are modeled via bulk-flow theory of Hirs

$$\tau_{iz} = p w f_i, \quad \tau_{i\varphi} = p u_i f_i, \quad f_i = \alpha \frac{n_i}{2} (ph)^{m_i-1} |\mathbf{V}_i|^{m_i+1} (Re)^{m_i}, \quad |\mathbf{V}_i| = \sqrt{u_i^2 + w^2}, \quad (i = s, r) \quad (6)$$

where the subscript  $s$  is used for the stator surface,  $r$  is used for the rotor one; circumferential velocities relative to the stator and rotor are  $u_s = u$ ,  $u_r = u - U$  ( $U = \omega R$ ,  $R$  is the seal radius);  $n_i$  and  $m_i$  are empirical constants of Hirs' turbulent model. The equations (3)-(6) include dimensionless complexes: Strouhal number

$S = \frac{\omega L}{u_m}$ , Reynolds number  $Re = \frac{2\rho_m c_0 u_m}{\mu}$  ( $\mu$  is the gas viscosity,  $\rho_m = \frac{p_{in}}{u_m^2}$ ), the seal aspect ratio  $\beta = \frac{L}{2R}$ ,

parameter  $\alpha = \frac{L}{c_0}$ .

The flow through the seal is considered as isothermal [5].  
The entrance-loss equation ( $z=0$ ) is added as boundary condition

$$1 - p = \frac{1 + \xi}{2} p w^2 \quad (7)$$

and exit-recovery equation ( $z=1$ ) has the form

$$p - p_e = -\frac{1 - \eta}{2} p w^2 \quad (8)$$

Here  $\xi$  is the inlet pressure-loss coefficient (entrance-loss coefficient),  $\eta$  is the exit recovery coefficient (it was assumed that  $\eta=1$ ) and  $p_e$  is dimensionless sump pressure. The condition (8) is valid until the Mach number remains less than one for unchoked flow. If the Mach number at the exit reaches one for choked flow, the exit pressure remains different from the sump pressure and the condition (8) is not valid. In this case the condition  $w_1(1) = 0$  is used for the first-order equations instead of (8) (see next section). Also we specify the boundary condition for  $u$  (preswirl) at the point  $z=0$ .

### 3 SOLUTION PROCEDURE

#### 3.1 Perturbation analysis

Assuming small motion of the rotor about its geometric center, the pressure, axial velocity, circumferential velocity, and local seal clearance can be expanded in terms of zeroth-order and first-order perturbation variables

$$p = p_0 + \varepsilon p_1, \quad w = w_0 + \varepsilon w_1, \quad u = u_0 + \varepsilon u_1, \quad h = h_0 + \varepsilon h_1. \quad (9)$$

where  $\varepsilon = e/c_0$  is the eccentricity ratio. Special about our approach to the problem is the assumption that the inlet pressure-loss coefficient  $\xi$  depends on local seal clearance, which varies around the circumference. Hence, we write similar to (9)

$$\xi = \xi_0 + \varepsilon \xi_1,$$

where  $\xi_1$  is determined by the expression

$$\xi_1 = \left( \frac{\partial \xi}{\partial \varepsilon} \right)_0 = \left( \frac{\partial \xi}{\partial h} \right)_0 h_1.$$

Here the subscript "0" points out zero-eccentricity flow condition.

We now assume that the shaft is moving on a circular orbit around the centered position. Also  $h_1$  takes the form

$$h_1 = \cos(\varphi - \Omega t),$$

where  $\Omega$  is the whirl ratio, i. e. the ratio of the shaft whirl velocity to the shaft rotational velocity.

Substitution of these perturbed variables into the governing equations and the boundary conditions yield zero-order and first-order problems. Zero-order equations are nonlinear. They are numerically integrated using the Runge-Kutta method to obtain matched boundary conditions at the seal exit. First-order equations are linear. They are reduced to two Cauchy problems for a system of ordinary differential equations relative to functions dependent only on the axial coordinate  $z$ . These problems are solved by the Runge-Kutta method as well. The resulting forces on the shaft are calculated by perturbed pressure integration for a few discrete frequencies. We obtain the rotordynamic coefficients of (1) with use of least-square curvefits. All procedures are similar to those written in [5].

#### 3.2 Determination of the entrance-loss coefficient

The pressure drop in the entrance of the seal is caused by the flow separation on the front edge of the seal and subsequent eddy generation in the entrance region. It is less connected with the flow regime inside the seal. In this connection we will consider a plane annular seal with axial symmetry and smooth stator surface for the determination of the entrance pressure drop. The computation domain includes seal gap with adjoining areas as shown on the Figure 1. It is two-dimensional because of axial symmetry. In that whole domain we solve the Reynolds-averaged Navier-Stokes equations with  $k-\omega$  turbulence model. This model is fitted for simulation of wall-bounded flows with big lengthwise pressure drops. The inlet pressure  $p_{in}$  and the outlet pressure  $p_{out}$  are set respectively on the input and output boundaries of domain. No slip conditions are set on all walls (thick lines in Figure 1). The computations were performed with the help of FLUENT code.

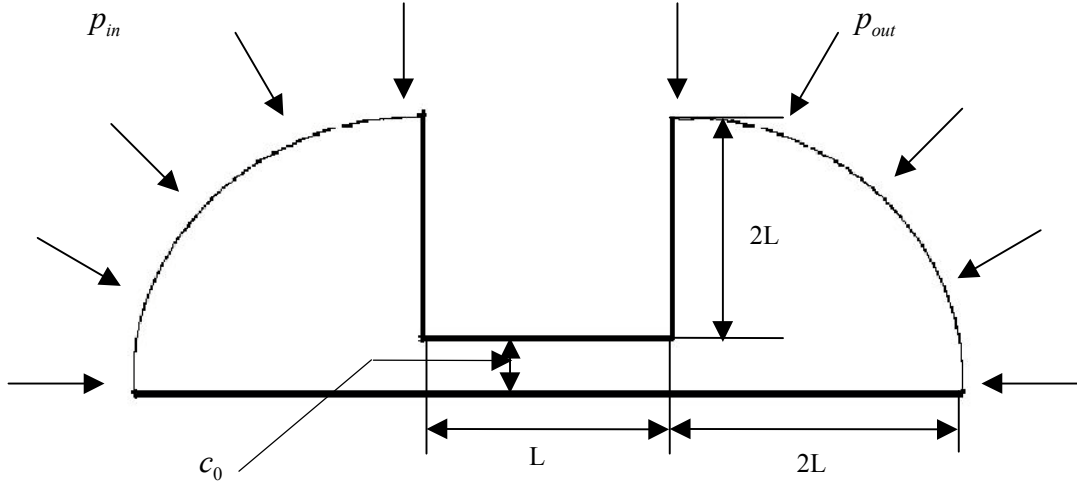


**Figure 1:** Seal gap with adjoining domains.

**Seal Data:**

Plane annular seal with axial symmetry and smooth stator surface

Gas: air

$$p_{in} = 8.26 \text{ bar}$$

$$p_{out} = 1.01 \text{ bar}$$

$$T = 302 \text{ K}^0$$

$$c_0 = 0.41 \text{ mm}$$

$$L = 50.8 \text{ mm}$$

$$D = 151.4 \text{ mm}$$

The derivative  $\left(\frac{\partial \xi}{\partial h}\right)_0$  was found using finite difference formula

$$\left(\frac{\partial \xi}{\partial h}\right)_0 = \alpha \xi(c_a) + \beta \xi(c_0) + \gamma \xi(c_b) \quad (10)$$

where  $\alpha = \frac{(H_b)^2 - (H_a)^2}{H_a H_b (H_a + H_b)}$ ,  $\beta = -\frac{H_b}{H_a (H_a + H_b)}$ ,  $\gamma = \frac{H_a}{H_b (H_a + H_b)}$  and  $H_a = c_0 - c_a$ ,  $H_b = c_b - c_0$ .

We take  $c_a = 0.3$  and  $c_b = 0.6$  as auxiliary values of clearance. The reason for this choice is the availability of data obtained by other authors (see [3]). These data were used for validation of the FLUENT computations.

The formula (10) has asymptotic precision of  $O(H^2)$ , where  $H = \max(H_a, H_b)$ . The dependence of the results from the value of  $H$  is the subject of further investigations.

We defined  $p$  and  $w$  from FLUENT calculation results as the average values in the entrance section of the seal. After that we find the entrance-loss coefficient  $\xi$  from (7) for given seal clearance. Very fine computational grid is needed for correct calculation of  $\xi$ . The computational grid with two hundreds of thousands nodes were used in our case. General structure of the computational grid is illustrated on Figure 2.

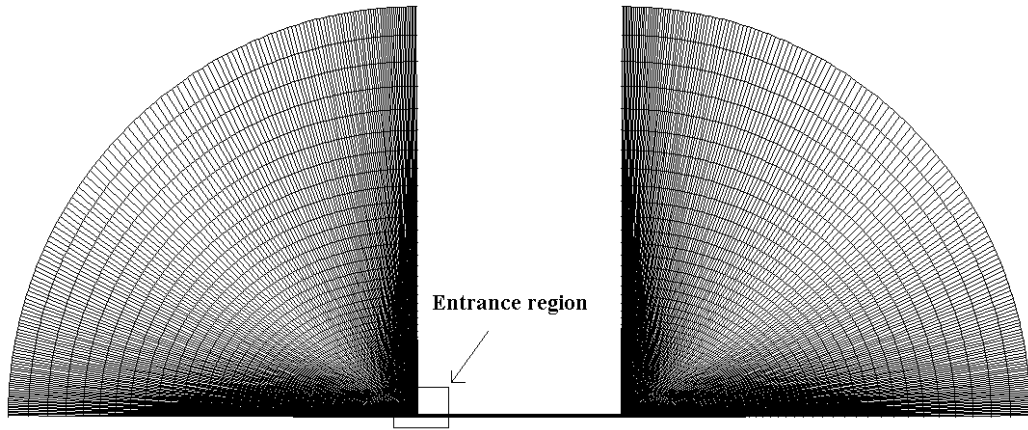


**Figure 2:** CFD computational grid.

The fragment of computational grid at the entrance region of the seal is illustrated on Figure 3.

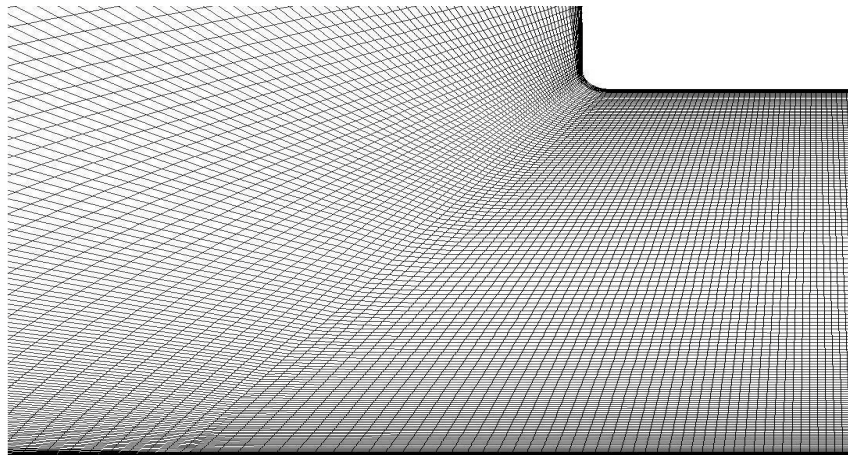


**Figure 3:** CFD computational grid (fragment)

#### 4 CALCULATION RESULTS

Figures 4 and 5 illustrate the pressure variation along the seal gap when Mach number at the exit of the seal is less than one or reaches one, respectively. Figure 4 corresponds to the case then  $p_{in}=7.8$  bar and  $p_{out}=3.5$  bar (unchoked flow). Figure 5 corresponds to the same seal geometry and  $p_{in}=8.26$  bar;  $p_{out}=1.01$  bar that leads to the choked flow. As we can see in Figure 4 for unchoked flow the exit pressure is equal to sump pressure  $p_{out}$ , otherwise (Figure 5) the pressure really has a “jump”. This “jump” is caused by the fact that the disturbance could not spread upstream when the flow velocity at the exit reaches the sonic velocity value. So the flow inside the seal does not “feel” the change of pressure at the reservoir.

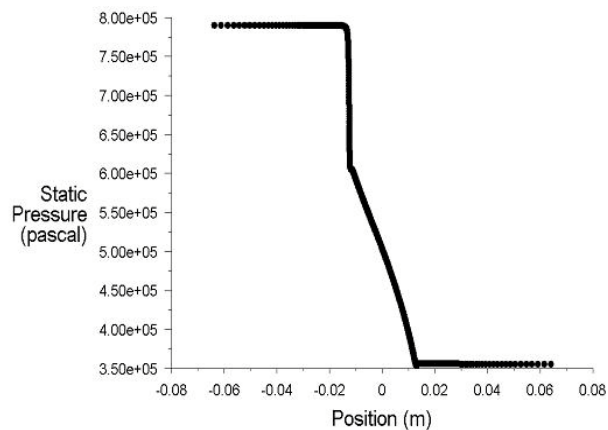


**Figure 4:** Pressure along the seal gap. (unchoked flow).

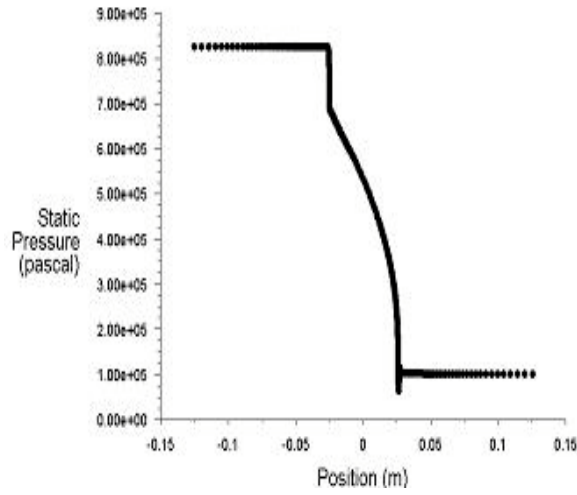


**Figure 5:** Pressure along the seal gap. (exit Mach number reaches one).

Figure 6 illustrates the velocity at the entrance section of the seal.

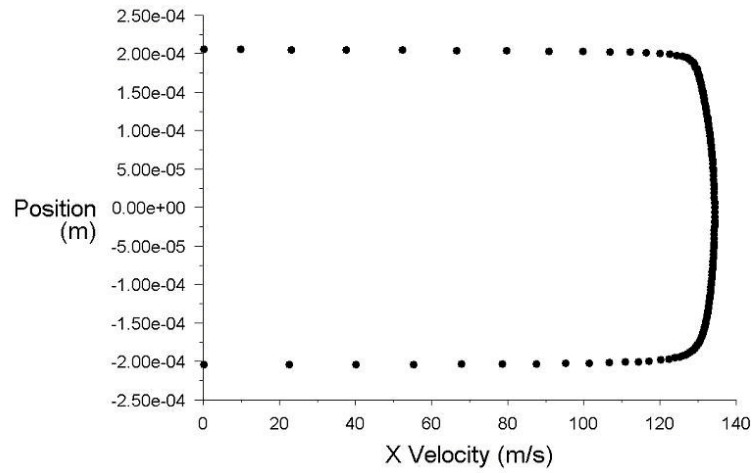


**Figure 6:** Velocity at the entrance section.

The values of entrance-loss coefficient  $\xi$  for diverse seal clearances are presented in Table 1.

**Table 1:** Entrance-loss coefficient for diverse seal clearances

$h$ (mm)	$\xi$
0,3	1,1941
0,41	1,2305
0,6	1,2983

Derivative  $\left(\frac{\partial \xi}{\partial h}\right)_0$  at  $c_0 = 0.41$  mm is equal to 0,3406.

Table 2 and Figure 7 show comparisons of predicted and experimental values of  $K$ . The experimental data (dots) were taking from the article [3].

In addition to the analysis described above we use the following seal data for the honeycomb seal [3]:

$$h_d = 1.91 \text{ mm}$$

$$m_r = -0.299, n_r = 0.154$$

$$m_s = -0.128, n_s = 0.295.$$

Here  $h_d$  is the honeycomb cell depth;  $n_i$  and  $m_i$  are empirical constants of Hirs' turbulent model.

We calculated the predicted values on two ways: with  $\xi=\text{const}$  (solid line) and with  $\xi = \xi(h)$  (dashed line).

**Table 2:** Relationship between direct stiffness and preswirl

Preswirl	K (N/mm)		
	Experiment [3]	$\xi=\text{const}$	$\xi=\xi(h)$
0	200	-259,78	215,21
0,2	—	-275,35	207,69
0,4	320	-275,41	211,07
0,6	—	-277,11	203,01
0,8	—	-278,24	200,18
1	340	-273,57	202,70

The same results are plotted in Figure 7

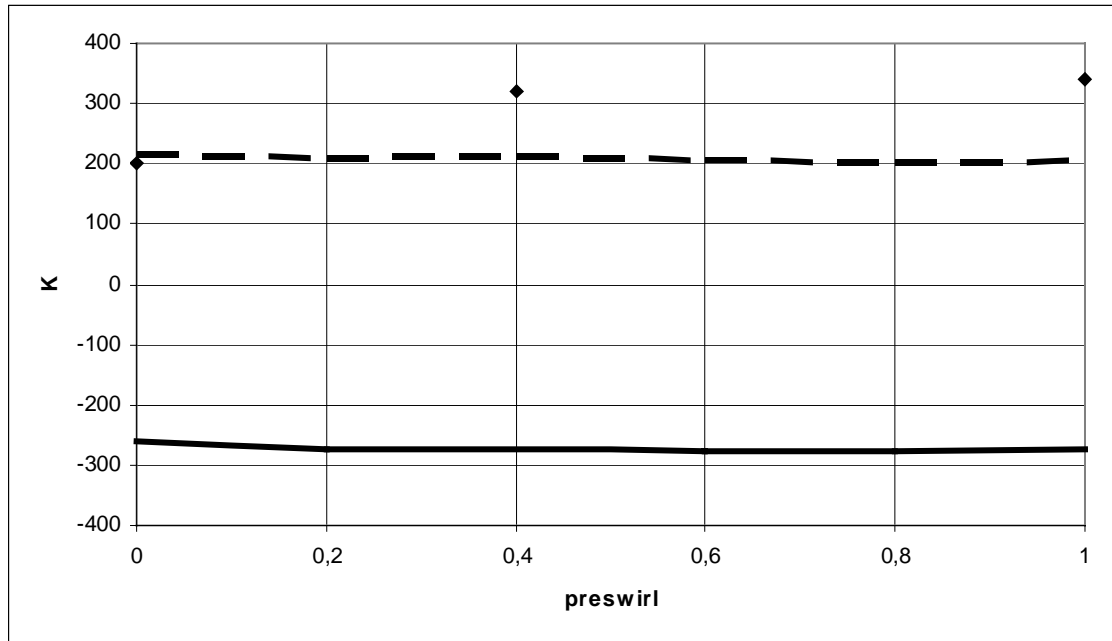


**Figure 7:** Direct stiffness as function of preswirl; experimental [3] (dots), constant entrance-loss coefficient (solid line), variable entrance-loss coefficient (dashed line); rotor speed 9500 cpm.

As we can see, taking into account the dependence  $\xi = \xi(h)$  in the seal model decreases the disagreement between experiment and numerical analysis. Possibly, the further improvement of this approach will allow even better agreement of the numerical results with experimental data. In particular, the optimization of the formula (10) has potential for further improvement.

The change of other rotordynamic coefficients due to dependence  $\xi = \xi(h)$  is about 5 percent.

## 5 CONCLUSION

This paper presents a new approach to seal analysis that combines bulk flow model with direct CFD simulation of the flow in the seal gap and surrounding areas. As a result we obtain much better coincidence of honeycomb seal direct stiffness with the experiment. This progress was made at the expense of a far more complicated analysis including accurate CFD simulations. On other hand this approach does not require 3-D simulation of the flow. Thus it does not need excessive computational resources such as multiprocessor computers.

## REFERENCES

- [1] Nelson C.C., "Rotordynamic Coefficients for Compressible Flow in Tapered Annular Seals," *ASME Journal of Lubrication Technology*, Vol. 107, Jul. 1985, pp. 318-325
- [2] Hirs G.G., "A Bulk Flow Theory for Turbulence in Lubricant Films," *ASME Journal of Lubrication Technology*, Vol. 95, No. 2, Apr. 1973, pp. 137-146
- [3] Elrod D.A., Childs D.W., Nelson C.C., "An Annular Gas Seal Analysis Using Empirical Entrance and Exit Region Friction Factors," *ASME Journal of Lubrication Technology*, Vol. 112, Apr. 1990, pp. 196-204
- [4] Ha, T. and Childs, D., 1992, "Friction-Factor Data for Flat-Plate Tests of Smooth and Honeycomb Surfaces," *ASME Journal of Tribology*, Vol. 114, pp. 722-729.
- [5] Kleynhans, G., and Childs, D., 1997, "The Acoustic Influence of Cell Depth on the Rotordynamic Characteristics of Smooth Rotor / Honeycomb Stator Annular Gas Seals", *ASME Journal of Engineering for Gas Turbines and Power*, Vol. 119, pp. 949-957.